
Analytical Solutions for Three-Dimensional Stability of Coastal Slope

C. Y. Han, X. H. Xia, and J. H. Wang

Abstract

The theory of limit analysis is presented for three-dimensional stability of coastal slope. In the frictional soils, the failure surface has the shape of logarithm helicoids, with outline defined by log-spirals. Dissipation rate and gravity power are obtained. By solving the energy balance equation, the expression of stability factor for coastal slope is obtained. The influences of the ratio of width and height and slope angle on the stability are evaluated. Numerical results are presented in the form of graphs. Some examples illustrate the practical use of the results.

Keywords

Stability • Landslides • Limit analysis • Coastal slope

1 Introduction

Coastal slope failures are major transport process from the upper slope to the ocean (Hutton and Syvitski 2004; Grilli et al. 2009; L'Heureux et al. 2010). Coastal slope failure can take different forms such as translational or rotational slides (Locat 2001). The different failure forms likely represent the different geotechnical and properties of the failed material, (Locat and Lee 2002; Tinti and Bortolucci 2000; Walters et al. 2006). In the absence of direct observations, scientists have made assumptions about failure institutions. The most common assumption is that a failure process is a cascade or an avalanche process (Densmore et al. 1998; Guzzetti et al. 2002; Malamud et al. 2004; McAdoo and Watts 2004; Lee and Stow 2007).

The stability of coastal slope has been given little attention in the past, even though coastal landslides are common. All coastal slope failures are three-dimensional 3D in practical, but two-dimensional 2D model is usually adopted with very simple. However, when the dimensions of coastal slope are clearly limited by adjacent rock formations or existing structures, a three-dimensional analysis of safety may be more appropriate (Ten Brink et al. 2009; Krastel et al. 2001; Locat et al. 2010).

The upper bound solutions for the failure of coastal slope are presented. The soil is treated as a plastic material, satisfying the coulomb's yield criterion. The failure surface has the shape of logarithm helicoids, with outline defined by log-spirals. Examples are provided to illustrate the stability factor influenced by the angle of internal friction, the unit weight of the soil, distance from sea level to slope top and slope width.

C. Y. Han (✉) · X. H. Xia · J. H. Wang
Department of Civil Engineering, Shanghai Jiaotong University,
Shanghai 200240, China
e-mail: hanyu02@163.com

X. H. Xia · J. H. Wang
Center for Marine Geotechnical Engineering, Shanghai Jiaotong
University, Shanghai 200240, China

2 Theoretical Formulation

The application of limit analysis to problems involving stability of earth slopes, first performed by Drucker and Prager (1952), involves determining a lower bound on the

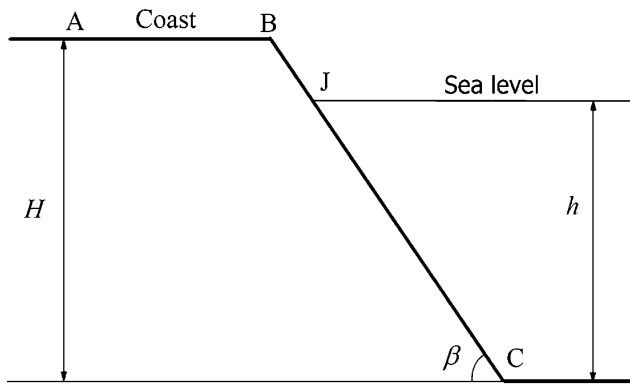
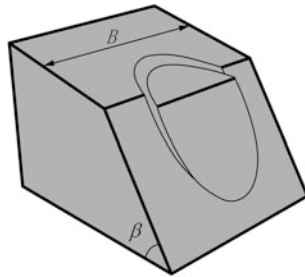


Fig. 1 Schematic diagram for coastal slope

Fig. 2 Three-dimensional rotational mechanism



collapse load by assuming a stress field which satisfies equilibrium and does not violate the yield criterion at any point. An upper bound is obtained by a velocity field compatible with the flow rule in which the rate of work of the external forces equals or exceeds the rate of internal energy dissipation.

The problem considered here is the safety factor of coastal slope with angle β as shown in Figs. 1 and 2. The upper-bound theorem of limit analysis states that the coastal slope will collapse, for any assumed failure mechanism, the rate of work done by the soil weight exceeds the internal rate of dissipation. Equating external and internal energies for any such mechanism thus gives an upper bound on the safety factor.

A rotational discontinuity mechanism is shown in Fig. 3, in which the failure surface is assumed to pass through the top and the toe of the coastal slope. Similar shape of this mechanism is considered by Michalowski and Drescher (2009) for evaluating critical height of slope. Soil over the failure surface rotates about the center of rotation O (as yet undefined), while the materials below the failure surface static. Failure surface AC is the velocity discontinuous surface. Assumed mechanism can be specified completely by three variables. For the sake of convenience, we select the angles θ_0 , θ_h and r'_0/r_0 . Equation for the logarithmic spiral surface is given by:

$$r = r_0 e^{(\theta-\theta_0) \tan \varphi}, \quad r' = r'_0 e^{-(\theta-\theta_0) \tan \varphi} \quad (1)$$

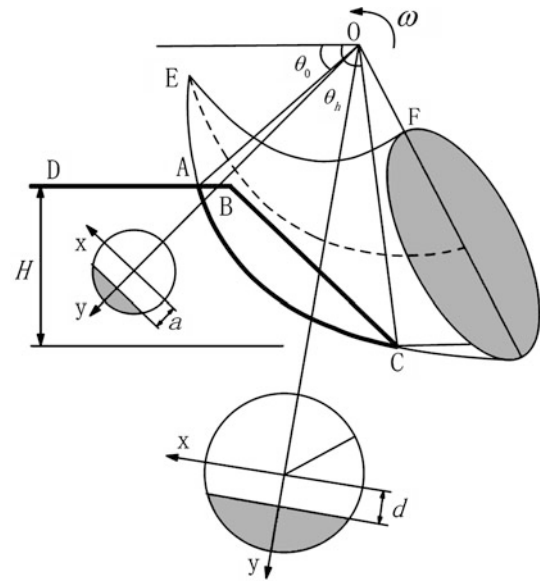


Fig. 3 Schematic diagram of the 3D mechanism

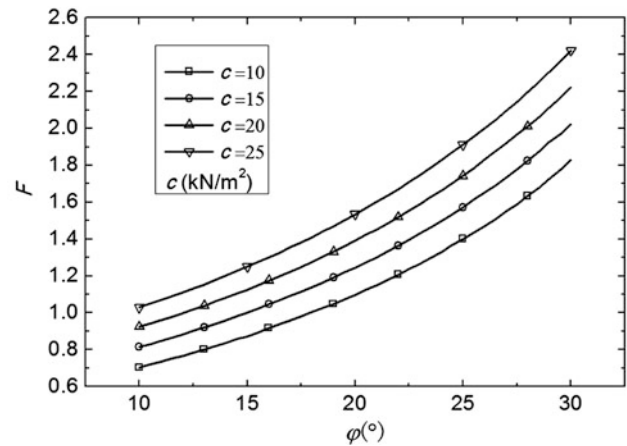


Fig. 4 Variation of safety factor F with the angle of internal friction

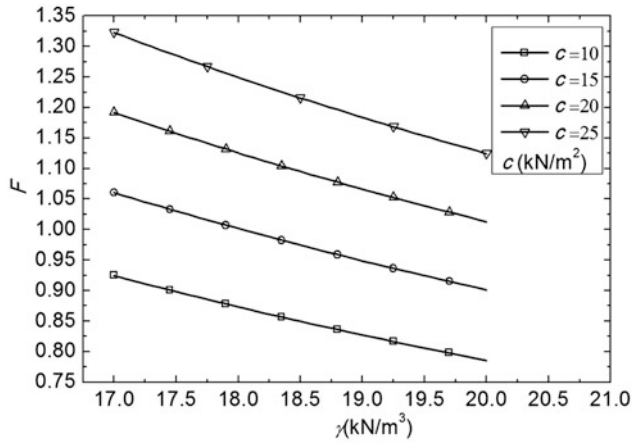
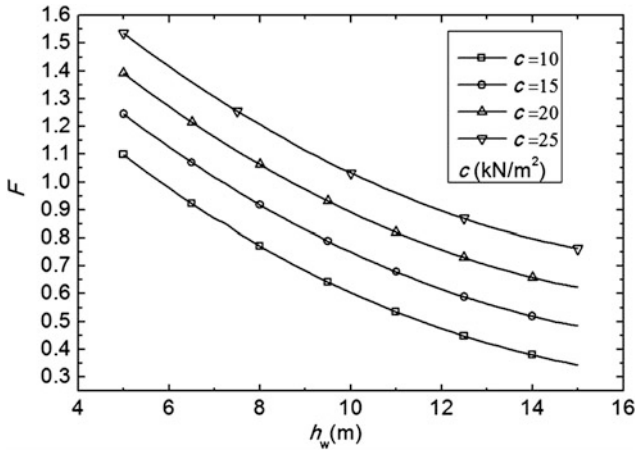
The rate of work of the external forces (weight) is:

$$W_\gamma = 2\omega\gamma \left[\int_{\theta_0}^{\theta_B} \int_0^{x_1^*} \int_a^{y^*} (r_m + y)^2 \cos \theta \, dy \, dx \, d\theta + \int_{\theta_B}^{\theta_h} \int_0^{x_2^*} \int_d^{y^*} (r_m + y)^2 \cos \theta \, dy \, dx \, d\theta \right] \quad (2)$$

where γ is unit weight of the soil, ω is angular velocity of the region ABC .

The total rate of external work due to the seawater pressure is.

$$W_w = -2\omega\gamma_w \int_{\theta_w}^{\theta_h} r_{x_2}^2 h'' \sqrt{R^2 - d^2} \cot(\theta + \beta) \, d\theta \quad (3)$$


Fig. 5 Variation of safety factor F with the unit weight of the soil

Fig. 6 Variation of safety factor F with distance from sea level to slope top

Internal dissipation of energy can be more specifically written as sum of integrals over top and surface of the coastal slope

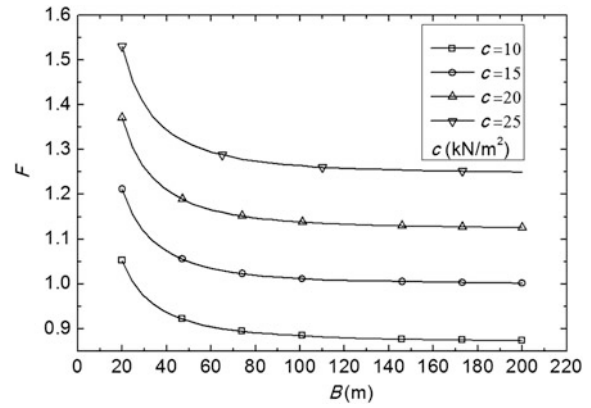
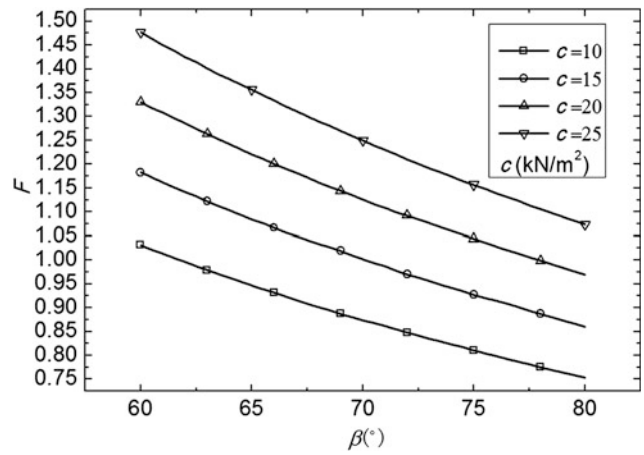
$$D = D_{AB} + D_{BC} \quad (4)$$

where the functions D_{AB} , D_{BC} are defined as:

$$\frac{D_{AB}}{c \cot \varphi} = -2\omega r_0^2 \sin^2 \theta_0 \int_{\theta_0}^{\theta_B} \frac{\cos \theta}{\sin^3 \theta} \sqrt{R^2 - a^2} d\theta \quad (5)$$

$$\begin{aligned} \frac{D_{BC}}{c \cot \varphi} = & -2\omega r_0^2 e^{2(\theta_h - \theta_0) \tan \varphi} \sin^2(\theta_h \\ & + \beta) \int_{\theta_B}^{\theta_h} \frac{\cos(\theta + \beta)}{\sin^3(\theta + \beta)} \sqrt{R^2 - d^2} d\theta \end{aligned} \quad (6)$$

where functions r_m , R , x_1^* , x_2^* , y^* , a , d , θ_B , r_{x_1} , r_{x_2} , r_{x_B} , h'' , θ_w are defined as:


Fig. 7 Variation of safety factor F with slope width

Fig. 8 Variation of safety factor F with slope angle

$$\begin{aligned} r_m = \frac{r + r'}{2}, R = \frac{r - r'}{2}, x_1^* = \sqrt{R^2 - a^2}, x_2^* = \sqrt{R^2 - d^2}, y^* \\ = \sqrt{R^2 - x^2}, \end{aligned}$$

$$a = \frac{\sin \theta_0}{\sin \theta} r_0 - r_m, d = \frac{\sin(\beta + \theta_h)}{\sin(\beta + \theta)} r_0 e^{(\theta_h - \theta_0) \tan \varphi} - r_m,$$

$$\begin{aligned} \theta_B = \arctan \frac{\sin \theta_0 \sin \beta}{\sin(\theta_h + \beta) e^{(\theta_h - \theta_0) \tan \varphi} - \sin \theta_0 \cos \beta}, r_{x_1} \\ = \frac{\sin(\beta + \theta_h)}{\sin(\beta + \theta_w)} r_0 e^{(\theta_h - \theta_0) \tan \varphi}, \end{aligned}$$

$$\begin{aligned} r_{x_2} = \frac{\sin(\beta + \theta_h)}{\sin(\beta + \theta)} r_0 e^{(\theta_h - \theta_0) \tan \varphi}, r_{x_B} \\ = \frac{\sin(\beta + \theta_h)}{\sin(\beta + \theta_B)} r_0 e^{(\theta_h - \theta_0) \tan \varphi}, \end{aligned}$$

$$h'' = r_{x_2} \sin \theta - r_{x_1} \sin \theta_w, \frac{r_{x_B}}{H - h} = \frac{\sin(\theta_w + \beta)}{\sin \beta \sin(\theta_w - \theta_B)}$$

The factor of overall safety is calculated as

$$F = \frac{D + W_w}{W_\gamma} \quad (7)$$

To avoid lengthy computations, these simultaneous equations may be solved by a numerical procedure. The minimum F_{\min} is calculated with independent variable parameters θ_0 , θ_h , r'_0/r_0 .

3 Example

Calculations for parameters are performed using the mechanisms in Fig. 3. For three-dimensional mechanisms, independent variable in minimising F is θ_0 , θ_h , r'_0/r_0 . Finding the least value of F requires a numerical procedure. In the procedure for finding the minimum of safety factor F , the independent variables, θ_0 , θ_h and r'_0/r_0 are changed sequentially by a single computational loop. The computational loop is repeated until the minimum is found.

The first example considers a coastal slope with the following parameters, slope depth 20 m, slope width 200 m, soil bulk density $\gamma = 18 \text{ kN/m}^3$, sea water density $\gamma_w = 10.22 \text{ kN/m}^3$, distance from sea level to slope top 5 m, and slope angle 70° . Figure 4 shows plots of F versus the angle of internal friction. The factor of safety increases as φ increases.

Figure 5 shows plots of F versus the unit weight of the soil with the following parameters, slope depth 20 m, slope width 200 m, the angle of internal friction $\varphi = 15^\circ$, sea water density $\gamma_w = 10.22 \text{ kN/m}^3$, distance from sea level to slope top 5 m, and slope angle $\beta = 70^\circ$. The factor of safety decreases with increasing soil bulk density

Figure 6 shows plots of F versus distance from sea level to slope top with the following parameters, slope depth 20 m, slope width 200 m, the angle of internal friction $\varphi = 20^\circ$, sea water density $\gamma_w = 10.22 \text{ kN/m}^3$, soil bulk density $\gamma = 18 \text{ kN/m}^3$, and slope angle $\beta = 70^\circ$. The factor of safety decreases with increasing h_w .

Figure 7 shows plots of F versus slope width with the following parameters, slope depth 20 m, soil bulk density $\gamma = 18 \text{ kN/m}^3$, the angle of internal friction $\varphi = 15^\circ$, sea water density $\gamma_w = 10.22 \text{ kN/m}^3$, distance from sea level to slope top 5 m, and slope angle $\beta = 70^\circ$. The chart shows that F is affected by slope width. The factor of safety decreases with increasing slope width.

>>Figure 8 shows plots of F versus slope angle with the following parameters, slope depth 20 m, soil bulk density $\gamma = 18 \text{ kN/m}^3$, the angle of internal friction $\varphi = 15^\circ$, sea water density $\gamma_w = 10.22 \text{ kN/m}^3$, distance from sea level to slope top 5 m, and slope width 200 m. The factor of safety decreases with increasing slope angle.

4 Conclusions

The upper bound method for the three-dimensional analysis of coastal slope stability is presented in this paper for frictional/cohesive soil. Formulas for the stability analysis are obtained through theoretical derivation on the basis of limit analysis theory. Rotational mechanisms are presented for coastal slope stability. The failure surface has the shape of logarithm helicoids, with outline defined by log-spirals.

Examples are provided to illustrate variations of the stability factor with the angle of internal friction, the unit weight of the soil, distance from sea level to slope top and slope width. The stability factor increases with decreasing the soil bulk density, distance from sea level to slope top and slope width. The safety factor increases as φ increases.

Acknowledgments This study was substantially supported by the grant from the National Natural Science Foundation of China (Grant No. 41172251, 41002095).

References

- Densmore, A. L., Ellis, M. A. et al. (1998). Landsliding and the evolution of normal-fault-bounded mountains. *Journal of Geophysical Research-Solid Earth*, 103(B7), 15203–15219.
- Drucker, D. C., & Prager, W. (1952). Soil mechanics and plastic analysis or limit design. *Quarterly of Applied Mathematics*, 10(2), 157–165.
- Grilli, S. T., Taylor, D. S., et al. (2009). A probabilistic approach for determining submarine landslide tsunami hazard along the upper east coast of the United States. *Marine Geology*, 264(1–2), 74–97.
- Guzzetti, F., Malamud, B. D., et al. (2002). Power-law correlations of landslide areas in central Italy. *Earth and Planetary Science Letters*, 195(3–4), 169–183.
- Hutton, E. W. H., & Syvitski, J. P. M. (2004). Advances in the numerical modeling of sediment failure during the development of a continental margin. *Marine Geology*, 203(3–4), 367–380.
- Krastel, S., Schmincke, H. U. et al. (2001). Submarine landslides around the Canary Islands. *Journal of Geophysical Research-Solid Earth*, 106(B3), 3977–3997.
- L'Heureux, J. S., Hansen, L., et al. (2010). A multidisciplinary study of submarine landslides at the Nidelva fjord delta, Central Norway—implications for geohazard assessment. *Norwegian Journal of Geology*, 90(1–2), 1–20.
- Lee, S. H., & Stow, D. A. V. (2007). Laterally contiguous, concave-up basal shear surfaces of submarine land-slide deposits (Miocene), southern Cyprus: differential movement of sub-blocks within a single submarine landslide lobe. *Geosciences Journal*, 11(4), 315–321.
- Locat, J. (2001). Instabilities along ocean margins: A geomorphological and geotechnical perspective. *Marine and Petroleum Geology*, 18(4), 503–512.
- Locat, J., Brink, U. S. T. et al. (2010). The block composite submarine landslide, southern New England Slope, USA: A Morphological Analysis.
- Locat, J., & Lee, H. J. (2002). Submarine landslides: advances and challenges. *Canadian Geotechnical Journal*, 39(1), 193–212.

- Malamud, B. D., Turcotte, D. L., et al. (2004). Landslide inventories and their statistical properties. *Earth Surface Processes and Landforms*, 29(6), 687–711.
- McAdoo, B. G., & Watts, P. (2004). Tsunami hazard from submarine landslides on the Oregon continental slope. *Marine Geology*, 203(3–4), 235–245.
- Michalowski, R. L., & Drescher, A. (2009). Three-dimensional stability of slopes and excavations. *Geotechnique*, 59(10), 839–850.
- Ten Brink, U. S., Barkan, R., et al. (2009). Size distributions and failure initiation of submarine and subaerial landslides. *Earth and Planetary Science Letters*, 287(1–2), 31–42.
- Tinti, S., & Bortolucci, E. (2000). Energy of water waves induced by submarine landslides. *Pure and Applied Geophysics*, 157(3), 281–318.
- Walters, R., Barnes, P., et al. (2006). Locally generated tsunami along the Kaikoura coastal margin: Part 2. Submarine landslides. *New Zealand Journal of Marine and Freshwater Research*, 40(1), 17–28.